Published in final edited form as:
Dev Neurobiol. 2012 April ; 72(4): 600–614. doi:10.1002/dneu.20955.

14-3-3 Proteins Regulate Retinal Axon Growth by Modulating ADF/Cofilin Activity

Byung C. Yoon[*], **Krishna H. Zivraj**, **Laure Strochlic**[†], and **Christine E. Holt**
Department of Physiology, Development and Neuroscience, University of Cambridge, Cambridge CB2 3DY, United Kingdom

Abstract

Precise navigation of axons to their targets is critical for establishing proper neuronal networks during development. Axon elongation, whereby axons extend far beyond the site of initiation to reach their target cells, is an essential step in this process, but the precise molecular pathways that regulate axon growth remain uncharacterized. Here we show that 14-3-3/14-3-3ζ proteins—adaptor proteins that modulate diverse cellular processes including cytoskeletal dynamics—play a critical role in *Xenopus* retinal ganglion cell (RGC) axon elongation *in vivo* and *in vitro*. We have identified the expression of 14-3-3/14-3-3ζ transcripts and proteins in retinal growth cones, with higher levels of expression occurring during the phase of rapid pathway extension. Competitive inhibition of 14-3-3/14-3-3ζ by expression of a genetically encoded peptide, R18, in RGCs resulted in a marked decrease in the length of the initial retinotectal projection *in vivo* and a corresponding decrease in axon elongation rate *in vitro* (30–40%). Furthermore, 14-3-3/14-3-3ζ (R1) co-localized with *Xenopus* actin depolymerizing factor (ADF)/cofilin (XAC) in RGC growth cones. Inhibition of 14-3-3/14-3-3ζ function with either R18 or morpholinos reduced the level of inactive pXAC and increased the sensitivity to collapse by the repulsive cue, Slit2. Collectively, these results demonstrate that 14-3-3/14-3-3ζ participates in the regulation of retinal axon elongation, in part by modulating XAC activity.

Keywords

growth cone; retinal ganglion cell; axon elongation; cytoskeleton; 14-3-3; ADF/cofilin

INTRODUCTION

Developing axons often travel a distance several magnitudes greater than the size of their soma to reach their target. In the embryonic *Xenopus* visual system, retinal ganglion cells (RGCs) extend axons through the optic pathway for distance of approximately 800 μm before reaching their synaptic target, the optic tectum. In the pathway, growth cones advance rapidly (around 60 μm/h), but when they reach the tectum, they stop advancing and begin arborizing (Harris et al., 1987) indicating that the dynamics of axon growth are highly regulated *in vivo*. Dynamic reorganization of actin and microtubules within growth cones are thought to underlie axon elongation (Letourneau, 2009). The retrograde flow of actin at the leading edge of the growth cone prevents the invasion of microtubules into the peripheral domain (P-domain) and advancement of growth cone forward. When a growth

Correspondence to: Christine Holt (ceh@mole.bio.cam.ac.uk)..
[*] *Present address:* Johns Hopkins University School of Medicine, Baltimore, MD 21205, USA.
[†] *Present address:* Laboratoire des jonctions neuromusculaires normales et pathologiques, INSERM U686, France.

Europe PMC Funders Author Manuscripts

cone makes an adhesive contact with the substrate, formation of adhesion complexes, named "molecular clutches," stop the actin retrograde flow, allowing microtubules to advance forward and leading to axon elongation (Giannone et al., 2009; Letourneau, 2009).

Increasing evidence suggests that actin depolymerizing factor (ADF) and cofilin play a critical role in regulating actin dynamics and axon growth. ADF/cofilins are highly expressed in neuronal growth cones, particularly in areas of high rate of actin disassembly (Bamburg and Bray, 1987; Svitkina and Borisy, 1999). Furthermore, overexpression of wild-type *Xenopus* ADF/cofilin (XAC) results in >50% increase in neurite length, possibly by disrupting actin filament and allowing microtubule-based extension (Meberg and Bamburg, 2000). ADF/cofilin was also shown to be critical for regulating cytoskeletal dynamics in response to extrinsic cues. For instance, brain-derived neurotropic factor (BDNF) acts via ADF/cofilin; activation of ADF/cofilin mimics the effect of BDNF on filopodial dynamics and its inhibition blocks the effect (Gehler et al., 2004). Similarly, a chemotropic response to bone morphogenic proteins (BMPs) and nerve growth factor (NGF), and netrin-1 were shown to involve ADF/cofilin (Wen et al., 2007; Marsick et al., 2010).

Previous studies also indicate that 14-3-3 (tyrosine 3-monooxygenase/tryptophan 5-monooxygenase activation) proteins are involved in the regulation of ADF/cofilin activity (Gohla and Bokoch, 2002). The 14-3-3 protein family consists of highly conserved, 30 kDa proteins with seven major isoforms named β, ε, γ, η, θ, σ, and ς (Bridges and Moorhead, 2005). 14-3-3 proteins are adaptor proteins with more than 100 binding partners that can directly regulate numerous molecular processes including inter- and intra-compartmental sequestration, activation/inactivation of enzymatic activity, and regulation of protein interactions (Muslin et al., 1996; Berg et al., 2003; Dougherty and Morrison, 2004; Aitken, 2006). Recent studies have shown that 14-3-3/14-3-3ς regulates actin dynamics by modulating the activity of ADF/cofilin. Direct interaction between cofilin and 14-3-3ς was demonstrated by yeast two-hybrid assays and GST pull-down experiments (Birkenfeld et al., 2003). Overexpression of 14-3-3ς in Cos-1 cells or BHK-21 cells increases inactive, phosphorylated cofilin (p-cofilin) levels by 10- to 13-fold and inhibits phosphatase2A-mediated de-phosphorylation of cofilin. Overexpression of 14-3-3ς also potentiates the LIMK-induced F-actin accumulation and clumping, presumably by decreasing the rate of cofilin-induced actin depolymerization (Gohla and Bokoch, 2002).

Microarray analysis of laser-captured growth cone mRNA previously identified the localization of transcripts with sequence shared by all 14-3-3 isoforms as well as sequence specific to the 14-3-3ς isoform (14-3-3/14-3-3ς), in retinal growth cones (Zivraj et al., 2010). Given their role in cytoskeletal dynamics, we asked whether 14-3-3/14-3-3ς plays a role in axon growth. Here we show that 14-3-3ς mRNA and protein are expressed in retinal growth cones and that the level of expression is developmentally regulated, positively correlating with the developmental stages when most of axon elongation occurs. Competitive inhibition of 14-3-3/14-3-3ς impaired axon growth *in vivo* and *in vitro* and was associated with a decreased level of inactive pXAC and increased sensitivity to Slit2. These results suggest that disrupted 14-3-3/14-3-3ς function leads to dysregulation of XAC activity and subsequent impairment in axon elongation.

MATERIALS AND METHODS

Xenopus Embryos

Female frogs were primed to lay with injection of pregnant mare serum gonadotropin (PMSG; Sigma) 1 week before they were induced to lay eggs by injection of 500 IUs of human chorionic gonadotropin (HCG; Sigma). Eggs were fertilized *in vitro* with

mechanically crushed male testes. Embryos were raised in 0.1X Modified Barth's Solution (MBS), at between 14 and 25°C to reach the desired stage, as determined by Nieuwkoop Pieter and Faber (1967).

Transformation, RT-PCR, and Morpholino Preparation

14-3-3 inhibitor R18-YFP (Difopein) and control R18K-YFP constructs were kind gifts from Dr. Haian Fu (Emory University, USA). Successfully transformed bacteria were selected using 1:1000 kanamycin plates. Amplified DNA was purified using Mini-prep (Qiagen) and/or Midi-prep (Qiagen) according to manufacturer's protocol and resolubilized in sterile ddH_2O. RT-PCR was performed with RNeasy micro kit (QIAGEN) using the following primers: 14-3-3ζ, forward 5′-CCCCTTCAGCTGTTATGGAG-3′, reverse 5′-ACTGGTTGGACAGGGACTTG-3′; β-actin, forward 5′-CGTAAGGACCTCTATGCCAA-3′, reverse 5′-TGCATTGATGACCATACAGTG-3′. Translational morpholinos with 3′FITC (GeneTools) were prepared in sterile ddH_2O. Morpholino sequences are as follows: 14-3-3ζ 5′-TCTGGACCAGTTCATTTTTATCCAT-3′; control 5′-CCTCTTACCTCAGTTACAATTTATA-3′.

Blastomere Injection and Eye Electroporation

Blastomeres were injected at the eight-cell stage as described previously (Drinjakovic et al., 2010). The embryos were first de-jellied with 2% cysteine (Sigma) in 1X MBS, and CNS-fated, dorsal animal blastomeres were injected with 10 ng of morpholinos per blastomere, with the injection volume of 5 nL. After 24 h of injection, positively injected embryos were sorted by examining the expression of FITC-tagged morpholino.

Electroporation into the developing retina was performed as described (Falk et al., 2007). Stage 26–28 embryos were anesthetized using 0.04% MS222 in 1X MBS and placed into the custom-made, cross-shaped chamber. Flat-ended platinum electrodes (Sigma) were placed at each end of the transverse channels. Approximately 10–30 nL of morpholino and/or DNA solution was injected into the medial portion of the eye. The capillary was removed just before electric pulses were applied by the square wave pulse generator (TSS20 OVODYNE electroporator, Intracel; 8 pulses, 20 V, 50 ms long, 1 s apart).

Retinal Explant Culture and Growth Assay

For dissection, embryo jelly coats were removed with forceps, and embryos were washed in 0.1X MBS+PSF. Embryos were anesthetized and dissected in a 1:1 mixture of culture medium and MS222 solution (0.4 mg/ml 3-aminobenzoic acid ethyl ester methanesulfonate salt (Sigma). The eye primordia were dissected out at stage 32, washed in culture medium, and then plated on laminin-coated glass cover slips. Cultures were grown at 20°C for 24–30 h. The rate of axon elongation was measured by imaging live cultures at 5 min intervals for 1 h total and determining the distance traveled by the growth cone, specifically the central domain, between each time point. Nikon TE2000-U microscope was used with phase optics, 100X or 60X objectives and a Nikon C-SHG1 mercury lamp. Neutral density filters were inserted to minimize phototoxicity.

Dissociated Retinal Cell Culture

Eyes from stage 26–28 embryos were dissected as described above and trypsinized for 6 min until the reaction was stopped using 60% L-16/10% FBS (GIBCO). Trypsinized eyes were then mechanically dissociated by pipetting up and down with a flame-pulled Pasteur pipette (tip diameter 100–150 μm). Dissociated cells were then plated onto laminin-coated cover slips and cultured at 60% L-16/10% FBS at 20°C for 24–30 h.

Collapse Assay

Retinal explant cultures were stimulated with Slit2 from transfected cell culture expressing Slit2 (Culture media; CM; kind gift from Dr Erhard Hohenester, Imperial College, London). For stimulation, Slit2 CM was added to the retinal culture at 1:1.14 dilution. Slit2 CM stimulation resulted in a mean collapse rate of 80%. Sub-threshold Slit2 CM was prepared by diluting Slit2 CM 1:2 with culture medium before adding them to the retinal culture. The sub-threshold concentration was determined by serial dilution of Slit2 CM and collapse assays; the concentration at which Slit2 stimulation did not cause significant collapse (<30% collapse rate) was used. Following stimulation, cultures were fixed in 2% PFA and 7.5% sucrose for 30 min. They were then washed three times with PBS. Growth cones with no lamellipodia and ≤2 filopodia, each shorter than 10 μm were classified as collapsed. All counts of collapsed growth cones were performed blind to the experimental condition to avoid subjective bias.

In Situ Hybridization of Growth Cones Using Digoxigenin (DIG)-Labeled Probes

The DIG-labeled riboprobes were made from *Xenopus* 14-3-3ζ IMAGE clone (No. 3869494) as described (Blichenberg et al., 1999). Fluorescence *in situ* hybridization (FISH) of cultured retinal GC was performed as described (Blichenberg et al., 1999). *In situ* hybridization on retinal cryosections was performed as described (Mann et al., 2002).

Western Blot

Lysates for western blots were prepared using RIPA buffer (Sigma) containing 10% protease inhibitor cocktail (Sigma cat no. P8340; 1:1000). Protein samples were quantified using the Bradford assay (Biorad) and separated using a 10% polyacrylamide running gel in 0.5% Tris buffer. It was then transferred onto a membrane (Immobilon-PSQ Membrane, PVDF, 0.2 μm, 7 × 8.4 cm. Catalogue # ISEQ07850, Millipore) for overnight at 4°C in transfer buffer containing 16.7% EtOH. The membrane was blocked for 1–2 h in PBS with 10% milk and 0.2% Tween 20, incubated in primary antibody for 1–2 h at RT or overnight at 4°C in antibody solution (PBS with 5% milk and 0.05% Tween 20). Following the primary antibody incubation, the membrane was washed 3 times in wash solution (PBS with 1% milk and 0.2% Tween 20), incubated in a secondary antibody conjugated to HRP in the antibody solution for 45 min, and washed 3 times. HRP was detected with ECL (Amersham) and X-ray film (Kodak). Antibodies used are as follows: 14-3-3 (Imgenex, rabbit, 1:1000); 14-3-3ζ (Genway, rabbit, 1:1000); α-tubulin (Abcam, mouse, 1:3000); HRP-conjugated goat anti-rabbit (Zymed, 1:10,000); and HRP-conjugated, goat anti-mouse (Abcam, 1:10,000).

Immunofluorescence Staining and Image Analysis

Growth cones were fixed in 2% paraformaldehyde (PFA) and 7.5% sucrose, permeabilized in 0.5% Triton X-100, and blocked in 5% heat-inactivated goat serum. Growth cones were incubated in primary antibody (in 5% heat-inactivated goat serum) for 1–3 h at room temperature or overnight at 4°C and with a secondary antibody (in 5% heat-inactivated goat serum) for 45 min. Stained samples were mounted using FluorSave (Calbiochem) and imaged on a Nikon TE2000-U microscope. For co-immunostaining using two antibodies from the same species, Zenon antibody conjugation kit (Invitrogen) was used according to manufacturer's instructions. pXAC (rabbit 1:500) and XAC (rabbit 1:500) antibodies were kind gifts from Dr. James R. Bamburg (Colorado State University, USA) (Abe et al., 1996). Other antibodies are as follow: 14-3-3 (Imgenex, rabbit, 1:100); 14-3-3ζ (Genway, rabbit, 1:100); Alexa 594-conjugated anti-mouse (Molecular Probes, goat, 1:1000); Alexa 488-conjugated anti-mouse (Molecular Probes, goat, 1:1000); Alexa 594-conjugate anti-rabbit

(Molecular Probes, donkey, 1:1000); Alexa 647-conjugate anti-rabbit (Molecular Probes, goat, 1:1000), Alexa 488-conjugated anti-rabbit (Molecular Probes, goat, 1:1000).

For quantitative immunofluorescence (QIF) analysis, a phase image was captured digitally followed by a fluorescent image for each growth cone. Identical gain and exposure settings were used for fluorescent image capture in each experimental trial, and care was taken to avoid pixel saturation. For signal intensity quantitation, the outline of the growth cone was traced on the phase image with a digital drawing pad and subsequently superimposed on the fluorescent-captured image and the mean fluorescence intensity per unit area was calculated digitally (OpenLab). The background value, calculated by placing the growth cone outline on an adjacent area of cell-free substrate, was subtracted to give the final value (mean signal intensity/unit area). Statistical analyses for QIF and all the other experiments described in the paper were performed using InStat software and were done blind to the experimental condition. For quantitative analysis of colocalization, Pearson coefficient of individual growth cones was measured using Volocity (Improvision).

RESULTS

14-3-3ς mRNA and Protein Expression in Retinal Growth Cones

Localization of 14-3-3/14-3-3ς to retinal growth cones was first indicated by previous microarray-based screens of *Xenopus* and mouse retinal growth cone mRNAs (Zivraj et al., 2010). To confirm the findings, we first performed RT-PCR of mRNAs purified from either head or eye lysates from *Xenopus* embryos/larvae and found that 14-3-3ς mRNA was present throughout different developmental stages. PCR-only amplification did not detect a signal, demonstrating that the detection of 14-3-3ς was not from genomic contamination [Fig. 1(A)]. To validate the localization of 14-3-3ς mRNA specifically in RGC growth cones, *in situ* hybridization (ISH) was performed on cultured axons and growth cones using DIG-labeled RNA probes. The antisense probe showed a high level of 14-3-3-ς transcript signal diffusely distributed in growth cones. The sense probe, used as a control, showed significantly less signal [Fig. 1(B, C)]. Furthermore, *in situ* hybridization of stage 40 larvae sections showed a strong 14-3-3ς signal in the retinal ganglion cell (RGC) layer as well as in the optic nerve head (ONH) where all the RGC axons collect to exit the eye [Fig. 1(D)]. The sense probe did not show a significant ISH signal, indicating that the RGC and ONH signals are specific [Fig. 1(D)]. These results demonstrate that 14-3-3ς mRNA localizes to RGC axons both *in vitro* and *in vivo*.

Next, the expression of 14-3-3/14-3-3ς proteins in retinal growth cones was examined using a pan-14-3-3 antibody and an isoform-specific 14-3-3ς antibody. The 14-3-3 pan-specific antibody is predicted to recognize all 14-3-3 isoforms and was used initially. The 14-3-3ς antibody is predicted to specifically recognize the ς isoform and its phosphorylated form, 14-3-3δ. Both antibodies gave a strong signal in head and eye lysates with western blot analysis [Fig. 2(A)]. The presence of specific bands at the expected molecular weight also confirmed the specificity of the antibody [Fig. 2(A)]. As predicted, the 14-3-3ς antibody recognized both phosphorylated and non-phosphorylated forms, which appear as a doublet [Fig. 2(A), low exposure inset]. Immunostaining of retinal growth cones confirmed the expression of 14-3-3/14-3-3ς, and revealed the punctate character of the signal distributed throughout the growth cone, including the filopodia [Fig. 2(B)]. These observations are consistent with expression of 14-3-3 proteins in dorsal root ganglion (DRG) axonal growth cones (Kent et al., 2010) and axonal proteomic analysis (Yoon and Holt, unpublished).

14-3-3ζ is Developmentally Down-Regulated

We next asked whether 14-3-3ζ expression is developmentally regulated. We hypothesized that if 14-3-3ζ were, indeed, involved in the regulation of axonal growth, its level would change to match demand depending on the level of axonal elongation in the embryo. For instance, expression may be high when retinal axons are actively elongating through the visual pathway (stages 27–39) and lower after axons reach their target, the optic tectum (stage 39/40). Such dynamic regulation of 14-3-3ζ expression is highly plausible given that growth cone sensitivity to guidance cues, like Sema3A and Slit2, is developmentally regulated through the receptor expression (Campbell et al., 2001; Piper et al., 2006). To test this possibility, retinal cultures from stage 24 embryos were grown for 8, 24, or 48 h—roughly corresponding to stages 28, 32, and 40 embryos, respectively—and subsequently immunostained for 14-3-3ζ. Since the size of retinal growth cones and the number of filopodia decrease with increasing developmental stage, we measured the mean signal intensity of 14-3-3ζ per unit area. The quantitative analysis of mean immunofluorescence intensity (QIF) revealed that the level of 14-3-3ζ in growth cones falls markedly (60%) by 48 h in culture, or stage 40 embryos (see Fig. 3), consistent with the hypothesis that the level of 14-3-3ζ in growth cones, indeed, decreases with time. Other molecules have shown to be upregulated in growth cones during similar time periods (e.g., Campbell et al., 2001; Zivraj et al., 2010), making it unlikely that this decrease simply reflects decreasing vitality.

Localization of 14-3-3ζ mRNA and protein in retinal growth cones as well as its developmentally regulated expression suggest that it may play a critical role in axon elongation. To test this possibility, we inhibited 14-3-3/14-3-3ζ activity using a specific, competitive inhibitor of 14-3-3/14-3-3ζ called R18 or difopein [Fig. 4(A)]. R18 consists of two peptides connected by a linker that competitively binds to all isoforms of 14-3-3, including 14-3-3ζ, and inhibits their interaction with target proteins (Wang et al., 1999; Masters and Fu, 2001). The R18 peptide has been shown to inhibit 14-3-3 function effectively in DRG growth cones and was found to alter axon guidance *in vitro* (Kent et al., 2010). As control, we used modified R18 with two arginines replaced by lysines, which does not bind to 14-3-3/14-3-3ζ [Fig. 4(A); R18K-YFP]. Both R18 and R18K were tagged with YFP to visualize axons expressing the peptides.

To assess the functional role of 14-3-3/14-3-3ζ *in vivo*, R18-YFP was electroporated into retinal precursor cells in eye primordia at stage 26, just before axonogenesis begins [Fig. 4(B)]. Examination of the retinotectal projection at stage 40 by visualization of YFP-expressing axons in wholemount brains revealed a severe shortening of R18-YFP projections with the majority of failing to extend beyond the mid-optic tract, and some barely reaching the midline chiasm, whereas control R18K-YFP projections all reached the tectum [Fig. 4(C)]. The projection length measured by tracing the YFP-positive axon trajectory from the optic chiasm to the longest axon tip [value “a” in Fig. 4(D)] was decreased by about 35% with R18-YFP [Fig. 4(D, E)]. As the decrease in pathway length may be secondary to a decrease in brain size, we also measured the ratio between the chiasm-to-axon tip [straight line value “b” in Fig. 4(D)] and the chiasm-to-posterior tectum [straight line value “c” in Fig. 4(D)]. The distance from the optic chiasm to the posterior tectum was not significantly different between the two conditions [Fig. 4(G)], signifying that the brain sizes are similar. Normalized to brain size, R18-YFP resulted in approximately 40% shorter pathway [Fig. 4(F)].

If the decrease in the pathway length in R18-YFP-expressing axons were, indeed, caused by reduction in the rate of elongation, the RGC pathway would be expected to form eventually at later stages. We thus examined the R18-YFP- or R18K-YFP-transfected embryos 2 days later at stage 43/44. At these later stages, the optic pathway length and brain size did not show any difference between the two conditions [Fig. 5(A–D)]. Of note, while R18-YFP

axons reached the tectum, they occasionally, exhibited unusual bends and tortuous trajectories or [Fig. 5(A)] suggestive of more subtle guidance defects during path finding.

To examine the role of 14-3-3/14-3-3ζ in axon growth more directly, we measured the axon elongation rate in retinal cultures after electroporation of R18-YFP or R18K-YFP. R18-YFP-expressing retinal cultures exhibited significantly shorter axons after 24 h of culture than controls [Fig. 5(E)]. For quantitative analysis, we conducted time-lapse imaging and calculated the elongation rate by measuring the displacement of the central domain of each growth cone during a 1-h period. The analysis showed a 30% decrease in the elongation rate in R18-YFP-expressing axons [Fig. 5(F)], demonstrating a direct effect on speed indicative of a role in regulating of axon growth *in vivo* and *in vitro*.

Decreased axon growth following 14-3-3/14-3-3ζ inhibition may have been caused by various mechanisms since 14-3-3/14-3-3ζ proteins are involved in diverse cellular processes. One possible mechanism is via disruption of XAC activity, given previous findings that 14-3-3/14-3-3ζ regulates XAC and that XAC activity is critical for proper axon growth (Meberg and Bamburg, 2000; Gohla and Bokoch, 2002). We first determined whether 14-3-3ζ colocalizes with XAC and pXAC in retinal growth cones. As both 14-3-3ζ and XAC antibodies are raised in rabbits, we first conjugated each antibody to different fluorophores, Alexa 488 and Alexa 594, before co-staining the growth cones. Immunofluorescence double staining revealed extensive co-localization of 14-3-3ζ with both XAC and pXAC [Fig. 6(A, B)], consistent with previous findings that 14-3-3ζ directly interacts with XAC in *Xenopus* (Lee et al., 2009). For quantitative analysis of co-localization, we measured Pearson coefficient of co-stained growth cones. Since the absolute value of Pearson coefficients can vary depending on analysis parameters, such as the region of interest and intensity threshold, we compared the relative value of Pearson coefficients in 14-3-3ζ/pXAC- or 14-3-3ζ/XAC-stained growth cones against those stained with unconjugated fluorophores, which non-specifically labeled the growth cones [Fig. 6(C)]. The mean Pearson coefficient in 14-3-3ζ/pXAC- or 14-3-3ζ/XAC-stained growth cones was significantly higher than in control [Fig. 6(D)], indicating that 14-3-3ζ and pXAC/XAC indeed co-localize.

Overexpression of 14-3-3ζ inhibits cofilin activity by directly binding to and protecting p-cofilin from dephosphorylation (Gohla and Bokoch, 2002). Based on this mechanism, pXAC would be expected to decrease when 14-3-3/14-3-3ζ function is inhibited. Therefore, we compared the pXAC levels in R18-YFP- and R18K-YFP-expressing growth cones using QIF analysis. With 14-3-3/14-3-3ζ inhibition, the pXAC level in RGC growth cones was reduced markedly (40%) whereas the level of total XAC was unchanged [Fig. 7(A, B)].

We next asked whether the reduction in pXAC levels in R18-YFP-expressing growth cones resulted from inhibition of the 14-3-3ζ isoform specifically, since R18 inhibits other isoforms of 14-3-3 as well. To test this, we injected a translation-blocking antisense morpholino (MO) against 14-3-3ζ into CNS-fated dorsal-animal blastomeres at the eight-cell stage. The injection allows the morpholino to be targeted to most RGCs and their axons/growth cones. The morpholino knockdown of 14-3-3ζ was around 35–40% effective as shown by western blot analysis of eye lysates and by QIF of 14-3-3ζ immunoreactivity in growth cones [Fig. 7(C, D)]. Similar to R18-mediated inhibition, the level of pXAC, but not total XAC, decreased significantly in MO-loaded growth cones [Fig. 7(E, F)]. These results suggest that the inhibition of 14-3-3/14-3-3ζ decreases pXAC in retinal growth cones, consistent with the idea that 14-3-3/14-3-3ζ normally represses XAC function, since phosphorylation inactivates XAC. Although our results do not rule out the possibility that other isoforms of 14-3-3 play a role in regulating XAC activity in growth cones, they indicate 14-3-3ζ is a key player in this process.

One implication of decreased pXAC following 14-3-3/14-3-3ζ inhibition is that XAC activity would be predicted to increase. Since Slit2-induced collapse stimulation involves upregulation of XAC (Piper et al., 2006), we reasoned that an increase in XAC activity (due to 14-3-3/14-3-3ζ inhibition) would be evident as an increased chemotropic response to Slit2. To test this hypothesis, we compared the Slit2 threshold response in 14-3-3-depleted and control growth cones using the growth cone collapse assay strategy reported by Wizenmann et al. (2009). We first determined the threshold and sub-threshold doses of Slit2 conditioned medium by serial dilution and collapse assays. Next, we stimulated R18-YFP- or R18K-YFP-expressing growth cones with the sub-threshold dose of Slit2. Stimulation of retinal cultures with sub-threshold Slit2 resulted in no significant collapse in cultures electroporated with control R18K-YFP (see Fig. 8). However, collapse increased greatly from 25 to 67% with sub-threshold Slit2 stimulation in cultures transfected with R18-YFP (see Fig. 8). This shows that R18-expressing growth cones are significantly more sensitive to Slit2 than controls and supports the idea that 14-3-3/14-3-3ζ inhibition increases XAC activity.

DISCUSSION

Many studies have focused on the role of 14-3-3/14-3-3ζ in adult tissues and cell lines (Aitken, 2006), but its role during nervous system development *in vivo* is not well characterized. Our findings show that loss of 14-3-3/14-3-3ζ causes abnormally short axonal projections during retinotectal pathway formation *in vivo* due to a slower rate in axon extension. Furthermore, our data provide evidence that suggests the effect on extension rate is mediated, at least in part, through changes in cofilin activity since 14-3-3/14-3-3ζ inhibition reduces the level of inactive phospho-XAC in growth cones and increases Slit2 sensitivity. The findings are consistent with previous studies showing that 14-3-3 binds directly to cofilin and down-regulates its activity and support a model in which high levels of 14-3-3 favor actin polymerization in growth cones and accelerate advancement (Gohla and Bokoch, 2002).

Previously, it has been shown that overexpression of wild-type XAC results in increased neurite growth (Meberg and Bamburg, 2000). The authors postulated that increased cofilin results in increased neurite outgrowth by disrupting the actin filament in growth cones, which assists microtubule-based extension. Although Meberg and Bamburg's study appears to contradict the findings described here, it is likely that axon growth requires an optimal ratio of pXAC and XAC. For instance, the same study showed that the increase in neurite outgrowth was markedly diminished when constitutively active (i.e., non-phosphorylated) cofilin mutant was expressed (Meberg and Bamburg, 2000). Expression of either constitutively active or dominant-negative Rac1 in *Drosophila* was also shown to cause defects in axon outgrowth (Luo et al., 1994). Since Rac1 activates LIMK1 which in turn inhibits cofilin by increasing p-cofilin level (Arber et al., 1998; Yang et al., 1998), it raises the possibility that axon outgrowth can be impaired when the balance between the levels of p-cofilin and cofilin is perturbed. When the cofilin/p-cofilin ratio is too high, for example, the actin dynamics may be tipped toward depolymerization, which may counteract the growth-promoting effect of increased microtubule extension into the P-domain. In line with this idea, treatment of chick DRG axons with cytochalasin B, which inhibits actin polymerization, severely impairs axon growth (Yamada et al., 1970). Similarly, cytochalasin B treatment of *Xenopus* RGC axons *in vivo* slows down axon growth (Chien et al., 1993). Examining the actin dynamics more directly in 14-3-3/14-3-3ζ inhibited growth cones may help elucidate this possibility. Furthermore, measuring the level of both pXAC and XAC in the same growth cones where 14-3-3/14-3-3ζ is inhibited may help elucidate this hypothesis further.

It is also possible that the effect of XAC disruption on axon growth following 14-3-3/14-3-3ζ inhibition was exacerbated by disruption of other cellular processes such as protein synthesis. For instance, 14-3-3 proteins, including the ζ isoform, were shown to bind and inhibit TSC (tuberous sclerosis), a protein that negatively regulates mTOR (target of rapamycin) activity (Liu et al., 2002; Nellist et al., 2003). In addition, overexpression of 14-3-3 increases phosphorylation of both S6K and 4E-BP1 in HEK293 cells, suggesting that increasing 14-3-3 activities leads to increased mTOR activity and translation (Li et al., 2002). Although the axon elongation rate is unaffected by short-term (1 h) inhibition of protein synthesis (Campbell and Holt, 2001), longer inhibition (>2 h) reduces axon elongation (Roche et al., 2009). Furthermore, a recent finding by Hengst et al. (2009) suggests that local protein synthesis is critical for NGF-induced axon elongation. Given these findings, it is possible that 14-3-3/14-3-3ζ also participates in the regulation of protein synthesis in retinal axons and growth cones and its inhibition may contribute to impaired axon growth partly by disrupted axonal protein synthesis.

Our results showed that retinal axons with inhibited 14-3-3/14-3-3ζ function still reach the tectum and, therefore, are able to navigate the pathway *in vivo*. This seems at odds with findings that suggest the role of 14-3-3/14-3-3ζ and ADF/cofilin in axon guidance. For instance, Kent et al. (2010) showed that expression of the same R18 inhibitor caused DRG axons *in vitro* to switch the polarity of their turning response to repellent gradients (MAG and NGF). As discussed previously, ADF/cofilin are also involved in a growth cone's response to chemotropic factors such as BDNF and netrin-1, implicating their role in axon guidance (Gehler et al., 2004; Marsick et al., 2010). Although the R18-YFP retinal axons did not appear to make large errors in path finding *in vivo*, the axons often showed abnormal loops and bends suggesting that guidance was more error-prone than normal. It is likely that additional compensatory mechanisms *in vivo* help to rescue errant axons, thus obscuring an obvious role in guidance. Interestingly, Kent et al. (2010) also showed that 14-3-3 proteins regulate levels of PKA in growth cones. Given that cAMP levels, like 14-3-3, are developmentally down-regulated in retinal growth cones (Höpker et al., 1999), it is tempting to speculate a causal link between the two.

Another interesting finding from the study is that 14-3-3/14-3-3ζ expression is developmentally regulated; its expression decreases markedly between 24 and 48 h in culture, equivalent to stage 32 and 40 embryos. As discussed previously, this regulation of 14-3-3/14-3-3ζ expression correlates with the phase of rapid axon elongation through the pathway *in vivo*. In addition, the responsiveness of retinal growth cones to guidance cues also changes over the course of development. For instance, young growth cones are not sensitive to Sema3A- or Slit2-induced collapse (stage 24) but gain responsiveness to these repulsive cues at later stages (stage 35/36) (Campbell et al., 2001; Piper et al., 2006). Results here also suggest that 14-3-3/14-3-3ζ inhibition increases response of growth cones to Slit2-induced collapse. Therefore, down-regulation of 14-3-3/14-3-3ζ expression in growth cones may contribute to the switching on of Slit2 sensitivity with developmental age. A plausible possibility is that 14-3-3ζ expression in growth cones is dynamically regulated, so that its highest expression level coincides with the initial period of axon elongation and is subsequently down-regulated to help slow down the axon growth and to reinforce the growth cone's responsiveness to repulsive cues at the optic tectum.

The presence of 14-3-3/14-3-3ζ mRNA in axons and growth cones suggests that its synthesis may be regulated locally. Indeed, mRNA localization provides a mechanism for fine spatial and temporal regulation of protein composition in subcellular compartments and can mediate stimulus-induced changes in axons and dendrites (e.g., Martin and Ephrussi, 2009; Yoon et al., 2009). Our preliminary results suggest that stimulation of growth cones with Slit2 or BDNF under repulsive conditions does not elicit local translation of 14-3-3ζ

(data not shown). However, more cues will need to be tested to address this issue. For example, *de novo* synthesis of 14-3-3/14-3-3ζ may be elicited by attractive guidance cues such as Netrin-1, which would then lead to a decreased level of active XAC. Furthermore, given the diverse function of 14-3-3/14-3-3ζ proteins, it is tempting to postulate that local synthesis of 14-3-3/14-3-3ζ may be an efficient way to fine-tune multiple cellular pathways within the growth cone.

Acknowledgments

This work was supported by a Wellcome Trust Programme Grant (CEH), Gates Cambridge Scholarship and Overseas Research Scholars Award (BY).

REFERENCES

Abe H, Obinata T, Minamide LS, Bamburg JR. *Xenopus laevis* actin-depolymerizing factor/cofilin: a phosphorylation-regulated protein essential for development. J Cell Biol. 1996; 132:871–885. [PubMed: 8603919]

Aitken A. 14-3-3 proteins: a historic overview. Semin Cancer Biol. 2006; 16:162–172. [PubMed: 16678438]

Arber S, Barbayannis FA, Hanser H, Schneider C, Stanyon CA, Bernard O, Caroni P. Regulation of actin dynamics through phosphorylation of cofilin by LIM-kinase. Nature. 1998; 393:805–809. [PubMed: 9655397]

Bamburg JR. Proteins of the ADF/cofilin family: essential regulators of actin dynamics. Annu Rev Cell Dev Biol. 1999; 15:185–230. [PubMed: 10611961]

Bamburg JR, Bray D. Distribution and cellular localization of actin depolymerizing factor. J Cell Biol. 1987; 105:2817–2825. [PubMed: 3320057]

Berg D, Holzmann C, Riess O. 14-3-3 proteins in the nervous system. Nat Rev Neurosci. 2003; 4:752–762. [PubMed: 12951567]

Birkenfeld J, Betz H, Roth D. Identification of cofilin and LIM-domain-containing protein kinase 1 as novel interaction partners of 14-3-3 zeta. Biochem J. 2003; 369:45–54. [PubMed: 12323073]

Blichenberg A, Schwanke B, Rehbein M, Garner CC, Richter D, Kindler S. Identification of a cis-acting dendritic targeting element in MAP2 mRNAs. J Neurosci. 1999; 19:8818–8829. [PubMed: 10516301]

Bridges D, Moorhead GB. 14-3-3 proteins: A number of functions for a numbered protein. Sci STKE. 2005; 2005:re10. [PubMed: 16091624]

Campbell DS, Holt CE. Chemotropic responses of retinal growth cones mediated by rapid local protein synthesis and degradation. Neuron. 2001; 32:1013–1026. [PubMed: 11754834]

Campbell DS, Regan AG, Lopez JS, Tannahill D, Harris WA, Holt CE. Semaphorin 3A elicits stage-dependent collapse, turning, and branching in Xenopus retinal growth cones. J Neurosci. 2001; 21:8538–8547. [PubMed: 11606642]

Chien CB, Rosenthal DE, Harris WA, Holt CE. Navigational errors made by growth cones without filopodia in the embryonic Xenopus brain. Neuron. 1993; 11:237–251. [PubMed: 8352941]

Dougherty MK, Morrison DK. Unlocking the code of 14-3-3. J Cell Sci. 2004; 117:1875–1884. [PubMed: 15090593]

Drinjakovic J, Jung H, Campbell DS, Strochlic L, Dwivedy A, Holt CE. E3 ligase Nedd4 promotes axon branching by downregulating PTEN. Neuron. 2010; 65:341–357. [PubMed: 20159448]

Falk J, Drinjakovic J, Leung KM, Dwivedy A, Regan AG, Piper M, Holt CE. Electroporation of cDNA/Morpholinos to targeted areas of embryonic CNS in Xenopus. BMC Dev Biol. 2007; 7:107. [PubMed: 17900342]

Gehler S, Shaw AE, Sarmiere PD, Bamburg JR, Letourneau PC. Brain-derived neurotrophic factor regulation of retinal growth cone filopodial dynamics is mediated through actin depolymerizing factor/cofilin. J Neurosci. 2004; 24:10741–10749. [PubMed: 15564592]

Giannone G, Mege RM, Thoumine O. Multi-level molecular clutches in motile cell processes. Trends Cell Biol. 2009; 19:475–486. [PubMed: 19716305]

Gohla A, Bokoch GM. 14-3-3 regulates actin dynamics by stabilizing phosphorylated cofilin. Curr Biol. 2002; 12:1704–1710. [PubMed: 12361576]

Harris WA, Holt CE, Bonhoeffer F. Retinal axons with and without their somata, growing to and arborizing in the tectum of Xenopus embryos: A time-lapse video study of single fibres in vivo. Development. 1987; 101:123–133. [PubMed: 3449363]

Hengst U, Deglincerti A, Kim HJ, Jeon NL, Jaffrey SR. Axonal elongation triggered by stimulus-induced local translation of a polarity complex protein. Nat Cell Biol. 2009; 11:1024–1030. [PubMed: 19620967]

Höpker VH, Shewan D, Tessier-Lavigne M, Poo M, Holt C. Growth-cone attraction to netrin-1 is converted to repulsion by laminin-1. Nature. 1999; 401:69–73. [PubMed: 10485706]

Kent CB, Shimada T, Ferraro GB, Ritter B, Yam PT, McPherson PS, Charron F, et al. 14-3-3 proteins regulate protein kinase a activity to modulate growth cone turning responses. J Neurosci. 1996; 30:14059–14067. [PubMed: 20962227]

Lee CW, Han J, Bamburg JR, Han L, Lynn R, Zheng JQ. Regulation of acetylcholine receptor clustering by ADF/cofilin-directed vesicular trafficking. Nat Neurosci. 2009; 12:848–856. [PubMed: 19483689]

Letourneau PC. Actin in axons: stable scaffolds and dynamic filaments. Results Probl Cell Differ. 2009; 48:65–90. [PubMed: 19582412]

Li Y, Inoki K, Yeung R, Guan KL. Regulation of TSC2 by 14-3-3 binding. J Biol Chem. 2002; 277:44593–44596. [PubMed: 12364343]

Liu MY, Cai S, Espejo A, Bedford MT, Walker CL. 14-3-3 interacts with the tumor suppressor tuberin at Akt phosphorylation site(s). Cancer Res. 2002; 62:6475–6480. [PubMed: 12438239]

Luo L, Liao YJ, Jan LY, Jan YN. Distinct morphogenetic functions of similar small GTPases: Drosophila Drac1 is involved in axonal outgrowth and myoblast fusion. Genes Dev. 1994; 8:1787–1802. [PubMed: 7958857]

Mann F, Ray S, Harris W, Holt C. Topographic mapping in dorsoventral axis of the Xenopus retinotectal system depends on signaling through ephrin-B ligands. Neuron. 2002; 35:461–473. [PubMed: 12165469]

Martin KC, Ephrussi A. mRNA localization: Gene expression in the spatial dimension. Cell. 2009; 136:719–730. [PubMed: 19239891]

Marsick BM, Flynn KC, Santiago-Medina M, Bamburg JR, Letourneau PC. Activation of ADF/cofilin mediates attractive growth cone turning toward nerve growth factor and netrin-1. Dev Neurobiol. 2010; 70:565–588. [PubMed: 20506164]

Masters SC, Fu H. 14-3-3 proteins mediate an essential anti-apoptotic signal. J Biol Chem. 2001; 276:45193–45200. [PubMed: 11577088]

Meberg PJ, Bamburg JR. Increase in neurite outgrowth mediated by overexpression of actin depolymerizing factor. J Neurosci. 2000; 20:2459–2469. [PubMed: 10729326]

Muslin AJ, Tanner JW, Allen PM, Shaw AS. Interaction of 14-3-3 with signaling proteins is mediated by the recognition of phosphoserine. Cell. 1996; 84:889–897. [PubMed: 8601312]

Nellist M, Goedbloed MA, Halley DJ. Regulation of tuberous sclerosis complex (TSC) function by 14-3-3 proteins. Biochem Soc Trans. 2003; 31:587–591. [PubMed: 12773161]

Nieuwkoop Pieter, D.; Faber, J. Normal Table of *Xenopus laevis* (Daudin): A Systematical and Chronological Survey of the Development from the Fertilized Egg Till the End of Metamorphosis. Garland Pub; New York: 1967.

Piper M, Anderson R, Dwivedy A, Weinl C, van Horck F, Leung KM, Cogill E, et al. Signaling mechanisms underlying Slit2-induced collapse of Xenopus retinal growth cones. Neuron. 1996; 49:215–228. [PubMed: 16423696]

Roche FK, Marsick BM, Letourneau PC. Protein synthesis in distal axons is not required for growth cone responses to guidance cues. J Neurosci. 2009; 29:638–652. [PubMed: 19158291]

Svitkina TM, Borisy GG. Arp2/3 complex and actin depolymerizing factor/cofilin in dendritic organization and treadmilling of actin filament array in lamellipodia. J Cell Biol. 1999; 145:1009–1026. [PubMed: 10352018]

Wang B, Yang H, Liu YC, Jelinek T, Zhang L, Ruoslahti E, Fu H. Isolation of high-affinity peptide antagonists of 14-3-3 proteins by phage display. Biochemistry. 1999; 38:12499–12504. [PubMed: 10493820]

Wen Z, Han L, Bamburg JR, Shim S, Ming GL, Zheng JQ. BMP gradients steer nerve growth cones by a balancing act of LIM kinase and Slingshot phosphatase on ADF/cofilin. J Cell Biol. 2007; 178:107–119. [PubMed: 17606869]

Wizenmann A, Brunet I, Lam JS, Sonnier L, Beurdeley M, Zarbalis K, Weisenhorn-Vogt D, et al. Extracellular engrailed participates in the topographic guidance of retinal axons in vivo. Neuron. 1996; 64:355–366. [PubMed: 19914184]

Yamada KM, Spooner BS, Wessells NK. Axon growth: roles of microfilaments and microtubules. Proc Natl Acad Sci U S A. 1970; 66:1206–1212. [PubMed: 5273449]

Yang N, Higuchi O, Ohashi K, Nagata K, Wada A, Kangawa K, Nishida E, et al. Cofilin phosphorylation by LIM-kinase 1 and its role in Rac-mediated actin reorganization. Nature. 1996; 393:809–812. [PubMed: 9655398]

Yoon BC, Zivraj KH, Holt CE. Local translation and mRNA trafficking in axon pathfinding. Results Probl Cell Differ. 2009; 48:269–288. [PubMed: 19343311]

Zivraj KH, Tung YC, Piper M, Gumy L, Fawcett JW, Yeo GS, Holt CE. Subcellular profiling reveals distinct and developmentally regulated repertoire of growth cone mRNAs. J Neurosci. 2010; 30:15464–15478. [PubMed: 21084603]

Europe PMC Funders Author Manuscripts

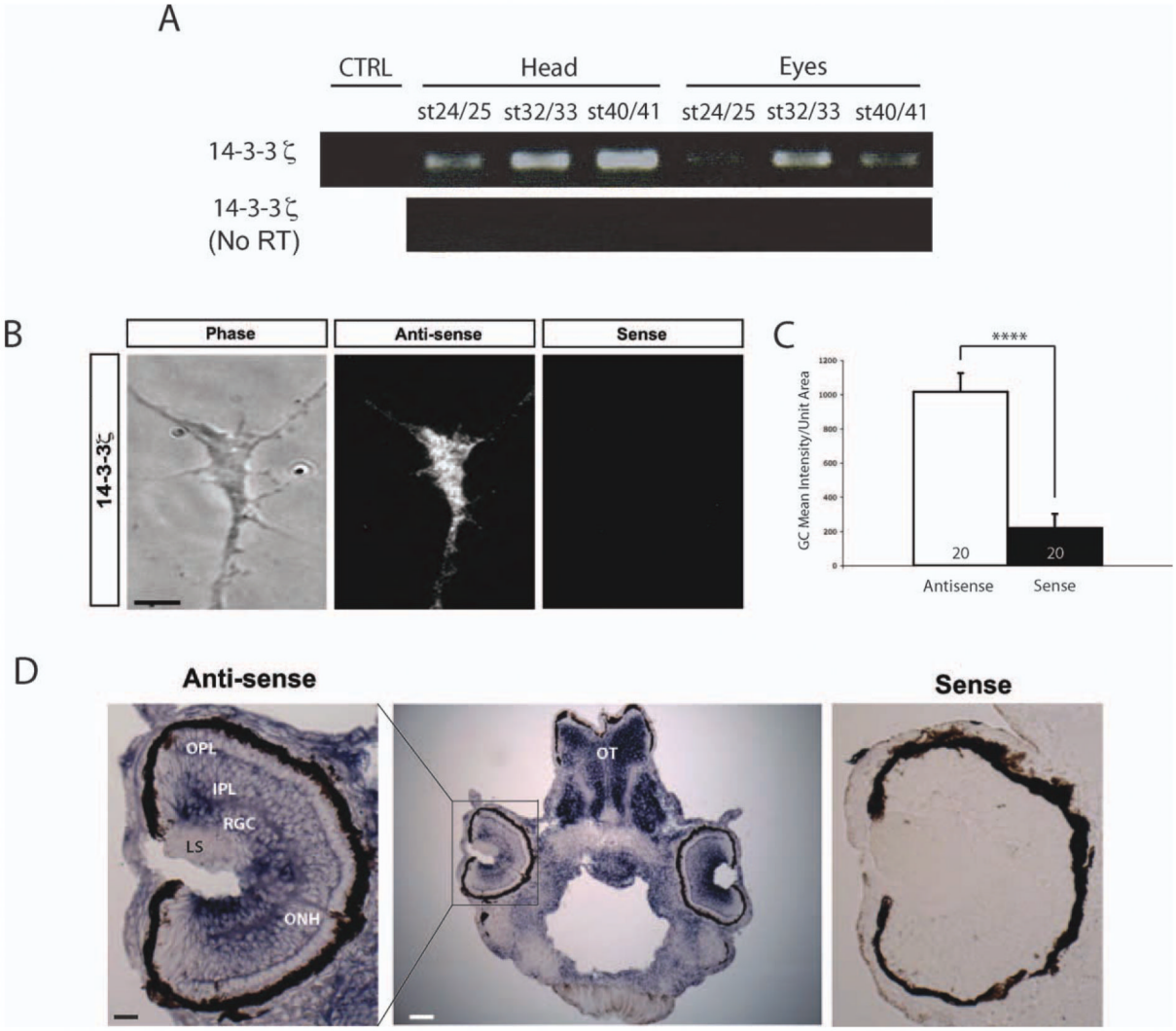

Figure 1.

Localization of 14-3-3ζ mRNA in retinal axons and growth cones. (A) RT-PCR of mRNAs purified from heads and eyes of various stages. RT only control was performed to rule out genomic contaminations. (B) Representative images of FISH with either anti-sense or sense probes (scale bar = 5 μm) (R1). (C) Quantification of FISH mean intensity per unit area (*n* = no. of growth cones; **** = $p<0.0001$; Mann–Whitney). (D) *In situ* hybridization of stage 40 embryo sections (ONH =optic nerve head, LS = lens, RGC = retinal ganglion cells, IPL = inner plexiform layer, OPL = outer plexiform layer, OT = optic tectum; scale bars = 25 μm for left panel and 100 μm for the middle panel). [Color figure can be viewed in the online issue, which is available at wileyonlinelibrary.com.]

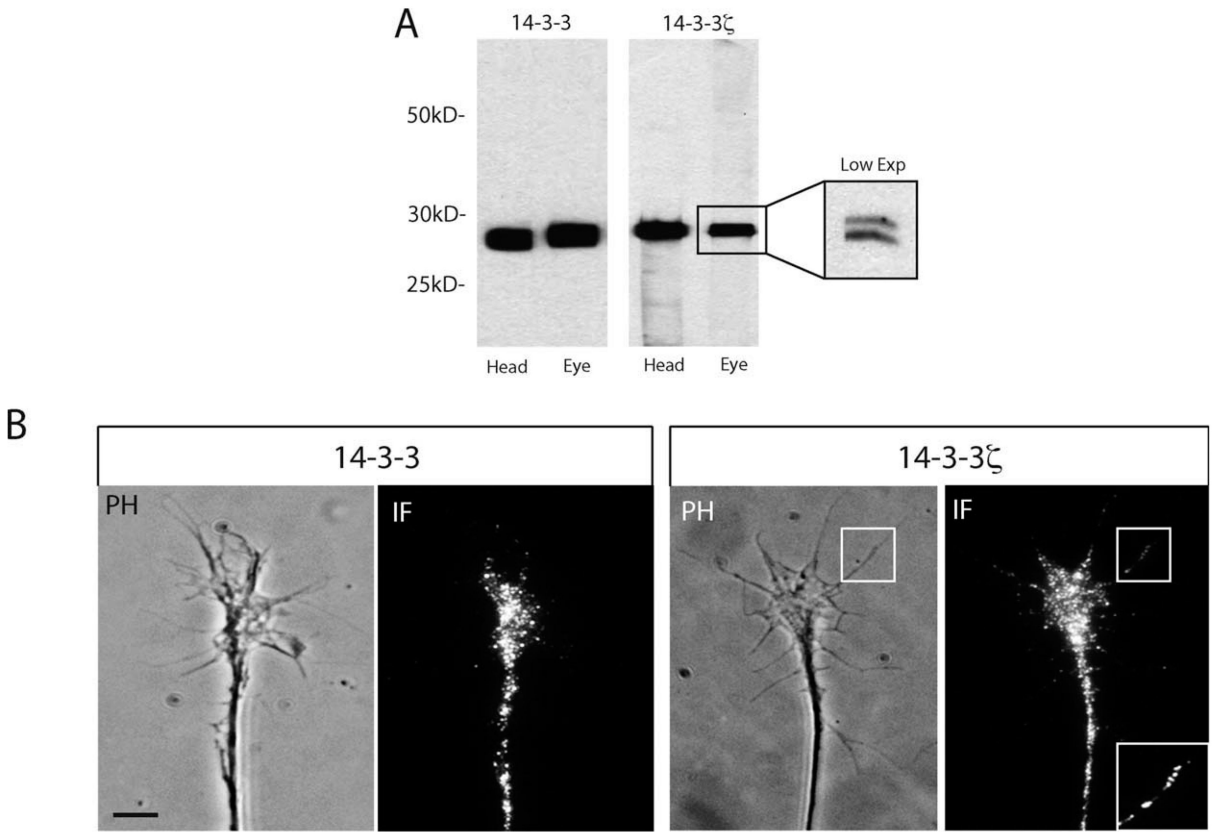

Figure 2.

14-3-3/14-3-3ζ proteins are expressed in retinal growth cones. (A) Western blot of head or eye lysates using 14-3-3 or 14-3-3ζ antibodies. The 14-3-3ζ antibody recognizes both the unphosphorylated and the phosphorylated form of 14-3-3ζ at a predicted molecular weight of ~ 29 kD (R1), which is more apparently visualized at low exposures (inset). (B) Immunofluorescence staining of retinal growth cones using 14-3-3 or 14-3-3ζ antibodies. The area marked by square shows localization of 14-3-3ζ within filopodia. A magnified view of the squared area is shown in the inset (scale bar = 5 μm).

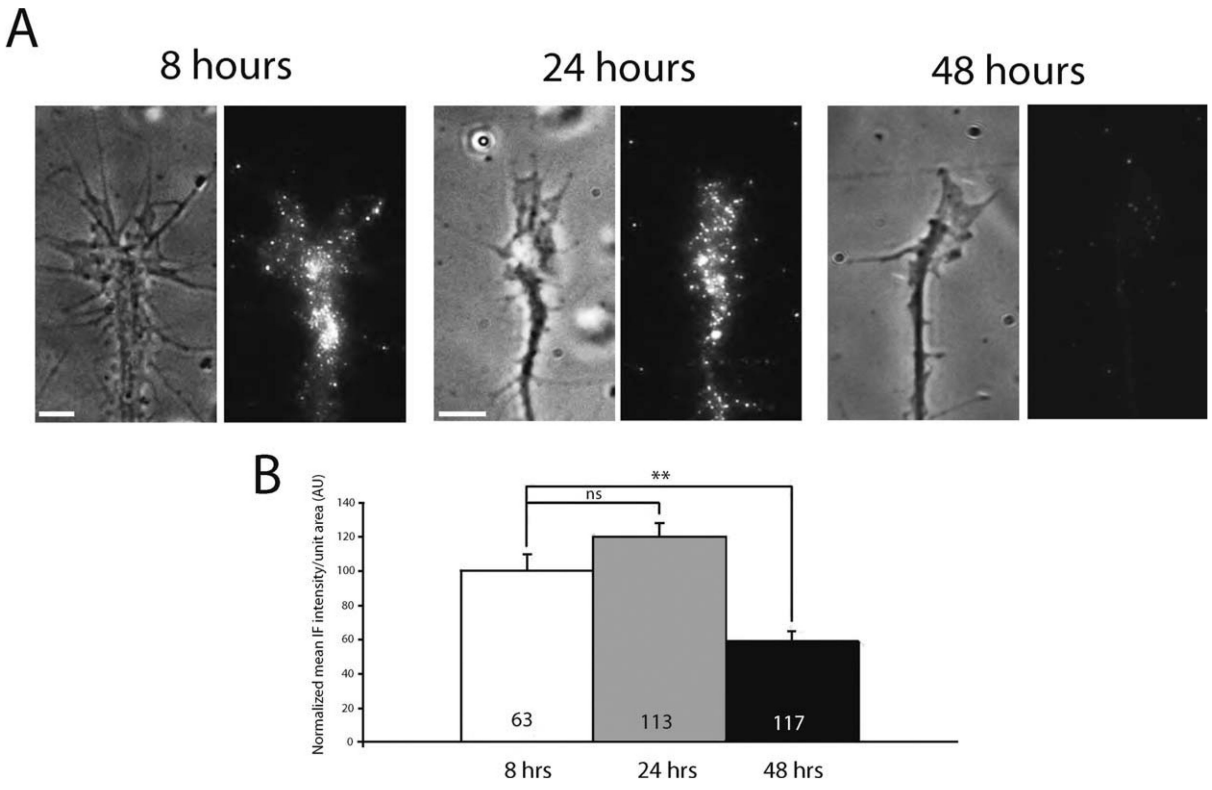

Figure 3.

The level of 14-3-3ζ in growth cones decreases with age. (A) Representative 14-3-3ζ IF staining in growth cones cultured for 8, 24, and 48 h (scale bars = 5 μm). (B) Quantitation of mean 14-3-3ζ IF intensity/unit area in growth cones cultured 8, 24, 48 h (*n* = no. of growth cones; three replicates; ** = $p<0.01$; one-way ANOVA with Bonferroni post-test).

Europe PMC Funders Author Manuscripts

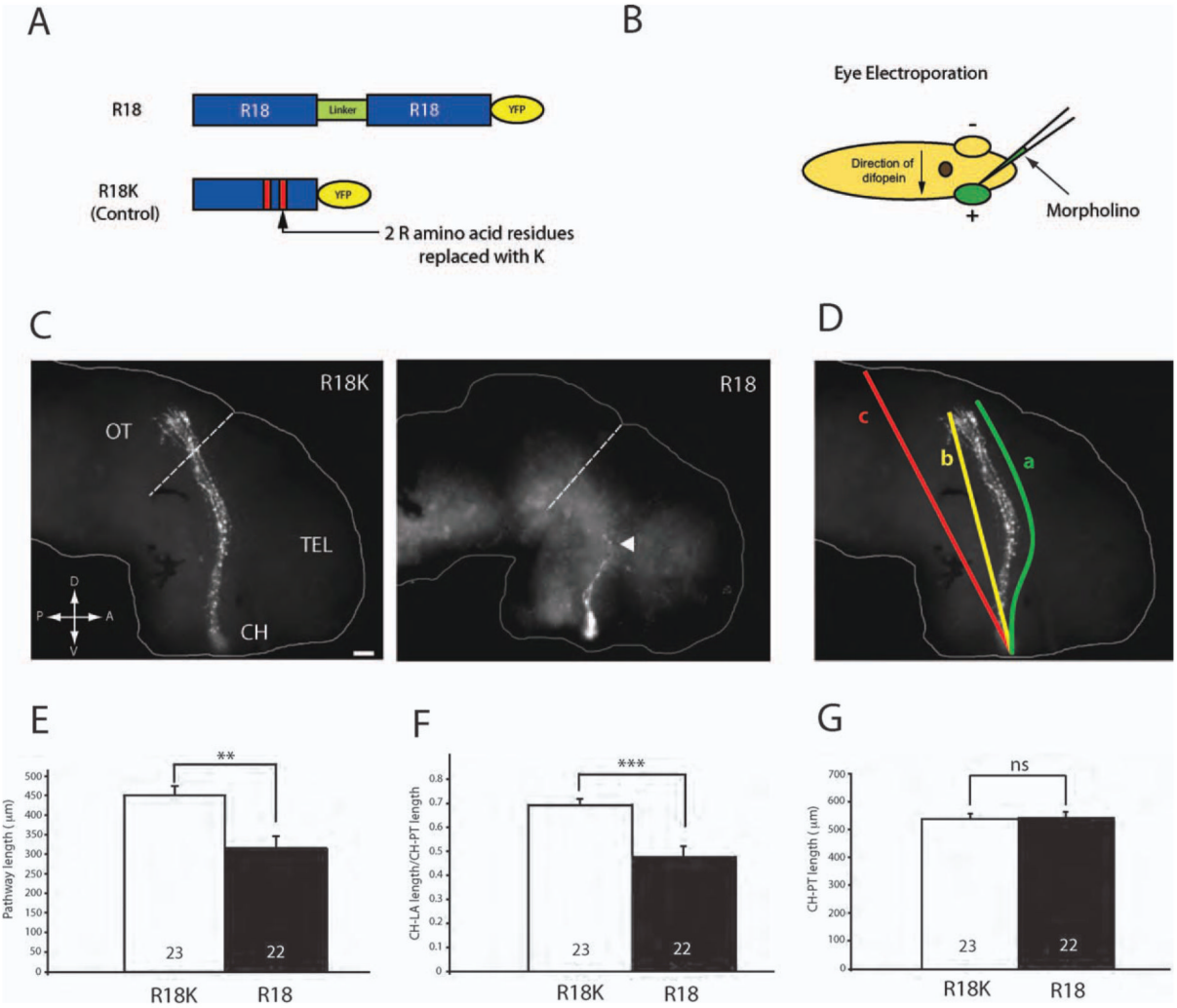

Figure 4.

Inhibition of 14-3-3/14-3-3ζ shortens retinal axon projection *in vivo*. (A) Schematics of R18 and R18K constructs tagged with YFP. (B) Schematics of eye electroporation. FITC-tagged morpholinos are electroporated into the eye at stage 26. (C) Dissected brains from stage 40 embryos that have been electroporated with either R18-YFP or R18K-YFP. The arrowhead indicates markedly shorter axons found in R18-YFP transfected brains (dashed line = anterior tectal border; scale bar = 50 μm; CH = optic chiasm; TEL = telencephalon; OT = optic tectum). (D) The length of the pathway was measured in two ways: (1) following the curvature of the pathway (a) and (2) measuring the shortest distance from the optic chiasm to the longest axon (LA; b) divided by the shortest distance from the chiasm to the posterior tectum (PT; c). (E) Measurement of the pathway length (equivalent to "a" in Fig. 4D). (F) Measurement of CH to LA length/CH to PT length (equivalent to "b/c" in Fig 4.4). (G) Measurement of CH to PT length to rule out significant differences in brain size. (Note: in E, F, and G, n = number of brains analyzed; three replicates; $^{**}p<0.01$; $^{***}p<0.001$; unpaired t-test).

Europe PMC Funders Author Manuscripts

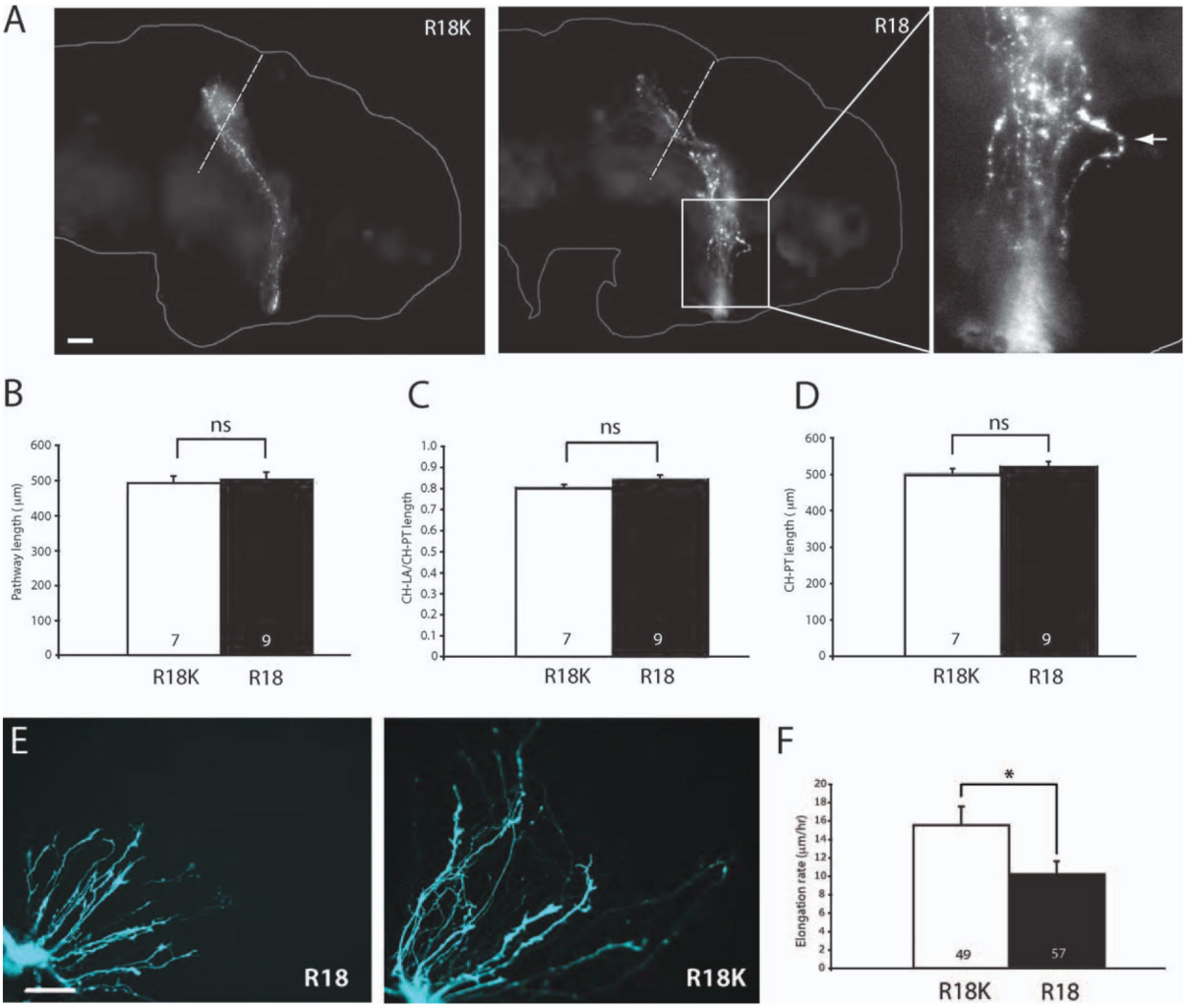

Figure 5.

Shortened retinal projection due to retarded axon elongation rate. (A) Brains of stage 43 embryos that have been eye-electroporated with R18-YFP or R18K-YFP (R1). Axons reach the tectum even in those that were electroporated with R18-YFP. The rightmost panel represents the magnified view of the R18 pathway with an axon taking an unusually tortuous path (arrowhead; dashed line = anterior tectal border; scale bar = 50 μm). (B) Measurement of the pathway length. (C) Distance from CH-LA/CH-PT. (D) Distance from CH-PT (For B, C, D, n = no. of brains analyzed; unpaired t-test). (E) Whole eye culture of eyes that have been electroporated with R18-YFP or R18K-YFP (scale bar = 50 μm). (F) The elongation rate of axons transfected with R18-YFP or R18K-YFP (n = no. of growth cones; *p<0.05; Mann–Whitney). [Color figure can be viewed in the online issue, which is available at wileyonlinelibrary.com.]

Europe PMC Funders Author Manuscripts

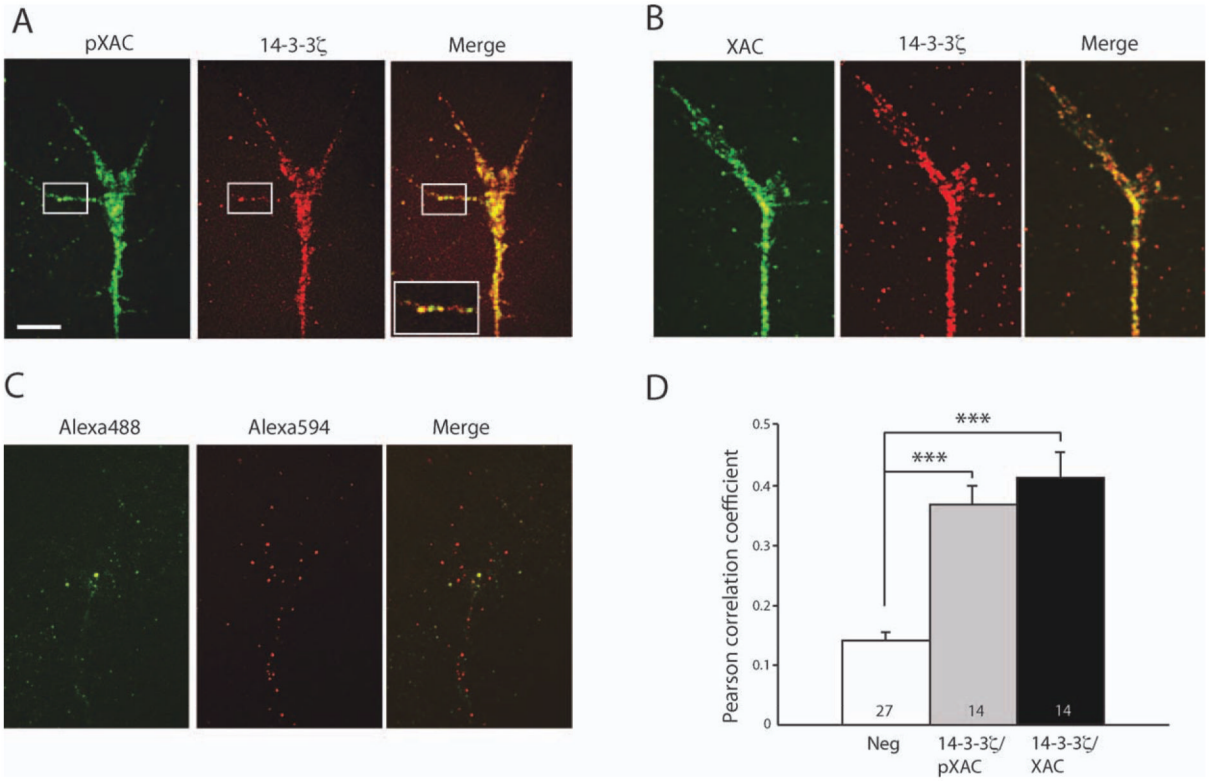

Figure 6.

Colocalization of 14-3-3ζ with pXAC and XAC. (A) Growth cone staining with Alexa 488-conjugated pXAC antibody and Alexa 594-conjugated 14-3-3ζ antibody. The squared area shows colocalization in a filopodium. The inset shows more magnified view of the squared area (scale bar = 5 μm; image intensity adjusted). (B) Growth cone staining with Alexa 488-conjugated XAC antibody and Alexa 594-conjugated 14-3-3ζ antibody. (C) Growth cone staining with Alexa 488 and Alexa 594 fluorophores without antibody conjugation. (D) Measurement of Pearson coefficient for determination of colocalization (n = no. of growth cones;***p<0.001; statistical analysis by Kruskal–Wallis test with Dunn post-test). (R1)

Europe PMC Funders Author Manuscripts

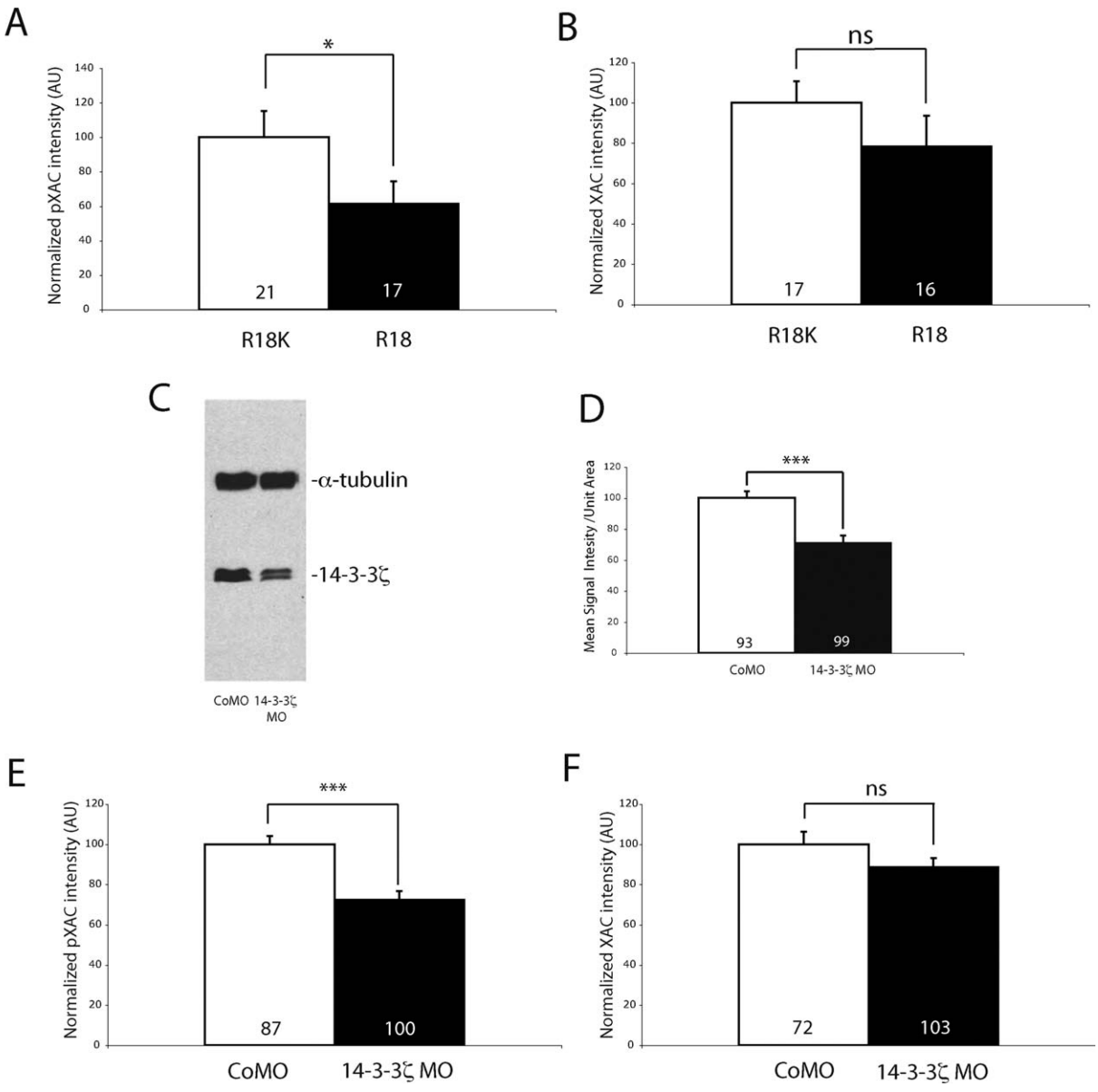

Figure 7.

14-3-3/14-3-3ζ knockdown decreases phospho-XAC in retinal growth cones. (A, B) QIF analysis of pXAC (A) and XAC (B) in growth cones transfected with either R18K- or R18-YFP (n = no. of growth cones; four replicates; *p<0.05; Mann–Whitney). (C) Western blot of eye lysates showing 14-3-3ζ knockdown with the antisense morpholino. α-Tubulin was used as a loading control. (D) QIF analysis of 14-3-3ζ in growth cones injected with either control or 14-3-3ζ morpholino (*** p<0.001; n = no. of growth cones; three replicates; unpaired t-test). (E, F) QIF analysis of pXAC (E) and XAC (F) in growth cones injected with control or 14-3-3ζ morpholino (n = no of growth cones; *** p<0.001; three replicates; unpaired t-test).

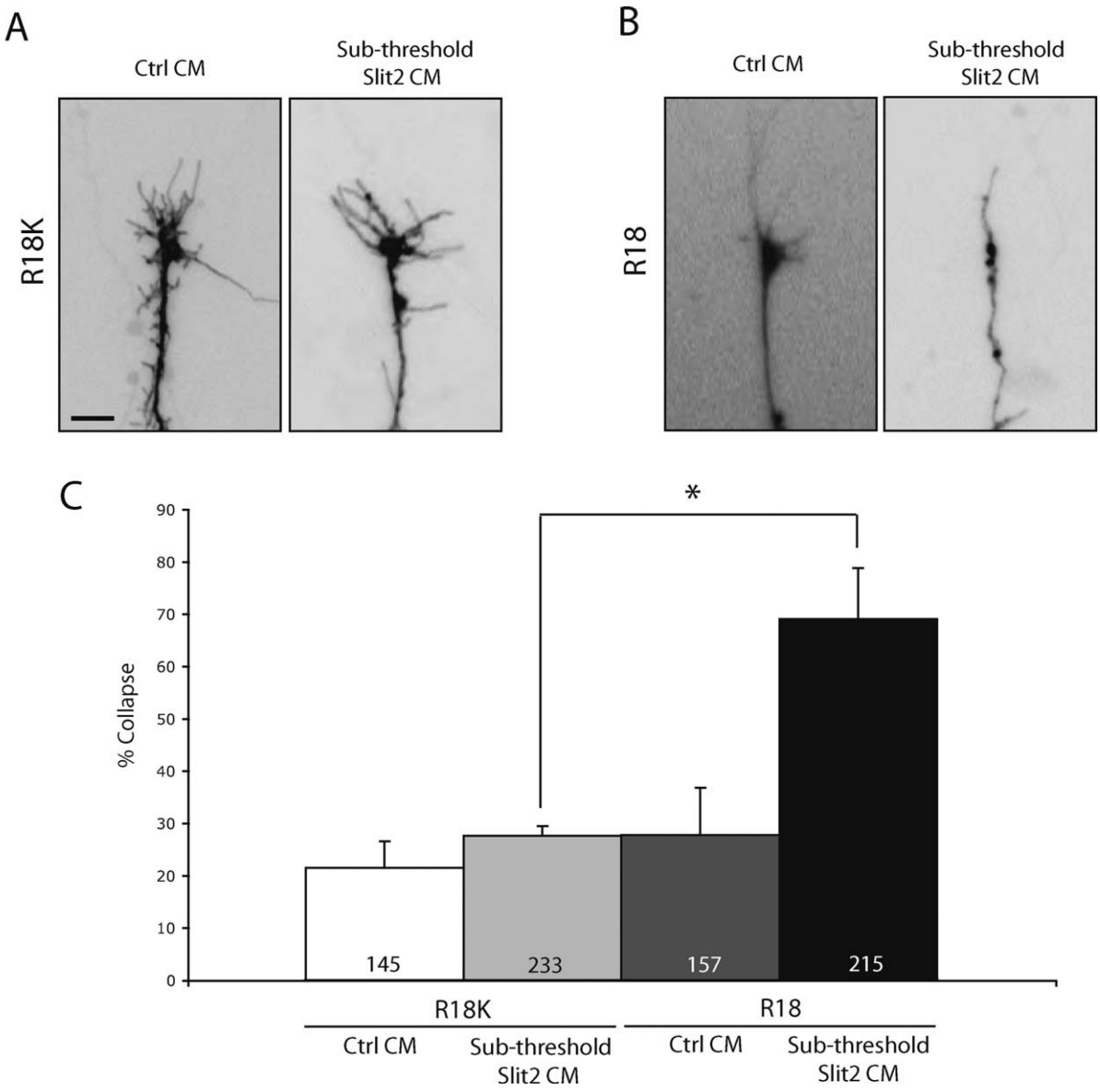

Figure 8.

14-3-3/14-3-3ζ inhibition sensitizes growth cones to Slit1-induced collapse. (A) R18K transfected growth cones stimulated with either control or Slit2 CM at sub-threshold concentration (scale bar = 5 μm). (B) R18-YFP transfected growth cones stimulated with either control or Slit2 CM at sub-threshold concentration. (C) Collapse rate of R18K- or difopein-transfected growth cones stimulated with either control or Slit2 CM at sub-threshold concentration (*n* = number of growth cones; three replicates; * = $p<0.05$; one-way ANOVA with Bonferroni post-test).